JOC The Journal of Organic Chemistry

Featured Article

pubs.acs.org/joc

Quantification of Nonstatistical Dynamics in an Intramolecular Diels–Alder Cyclization without Trajectory Computation

Debabrata Samanta, Anup Rana, and Michael Schmittel*

Department of Chemistry and Biology, Universität Siegen, Adolf-Reichwein-Strasse, D-57068 Siegen, Germany

Supporting Information

ABSTRACT: Experimental and computational (DFT) investigations reveal that enyne–allenes with an aryl group as probe at the allene terminus follow a dynamic non-IRC Diels–Alder cyclization pathway. Starting from two separate C^2–C^6 (Schmittel) transition states (TS), two distinct reaction paths originate that share a common diradical intermediate, however, without mixing! Because the momentum of the initial TS is transmitted into product formation, we suggest a simple protocol without trajectory computations to estimate the fraction of molecules that follow nonstatistical dynamics: It was calculated from the partitioning at the TSs, as derived from DFT computations, and the experimental ratio. The thus-determined percentage of dynamically reacting molecules only slightly depends on the depth of the intermediate well but rather on $\Delta\Delta G^{\ddagger}$ of the initial and the follow-up transition states.

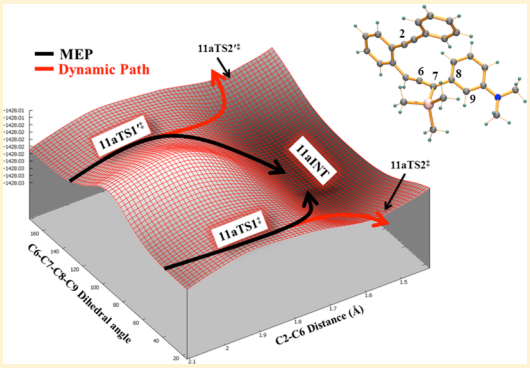

INTRODUCTION

The epitome of transition-state theory (TST)[1] is of central importance to chemists' understanding of selectivity in kinetically controlled chemical reactions. TST allows us to determine quantitatively the selectivity from the free energy difference $\Delta\Delta G^{\ddagger}$ of competing transition states (TSs). Another widely used method is RRKM theory,[2] which states that the energy obtained in a bimolecular collision has to be focused in the proper vibrational mode to cross the TS energy barrier. For multistep processes, the theory assumes that intramolecular vibrational energy redistribution (IVR) takes place much faster in the ensuing intermediate than crossing the next TS barrier. As a result, molecules usually relax in the intermediate state (if τ > 300 fs) and have to accumulate sufficient thermal energy one more time to populate reactive vibrational modes for crossing the next TS barrier. In contrast, once the reaction of an intermediate proceeds faster than IVR,[3] the selectivity of product formation is guided by nonstatistical dynamics and not by TST or RRKM theory.

Undeniably, an increasing amount of reactions involving S_N2 ion–dipole complexes,[4] organic diradicals,[5] radical cations,[6] radicals,[7] and others[8] have lately been identified to escape classical TST interpretations. In such circumstances, proving the occurrence of nonstatistical dynamics becomes very tedious and time-consuming because presently the scientific community requires detailed computational studies on the motions of atoms or groups along with extensive trajectory calculations at femtosecond-time resolution. While such a rigorous approach has its obvious merits, the complexity and time demands of trajectory calculations prevent any wider use within the community of mechanistic organic chemists.

In the past two decades, the C^2–C^6 (Schmittel) cyclization[9] has been a widely investigated reaction because of its utility for antitumor antibiotics[10] and intricate carbocycle[11] and heterocycle[12] formation. Lately, though, it has additionally moved into the focus of physical organic chemistry because the reaction outcome, so far documented for C^2–C^6/ene[5a,13] and C^2–C^6/Diels–Alder (DA) cyclizations,[14] often is not consistent with the common TST but needs to be discussed in light of nonstatistical dynamics.[5a,13,14]

Recent experimental evidence and DFT computational results obtained for the C^2–C^6/DA[14] cyclization of various enyne–allenes suggest that nonstatistical dynamic behavior depends on the substituents at both the alkyne and allene terminus. As an important experimental criterion for dynamic behavior, we utilize the temperature independence of the product ratio.[15] In the case of enyne–allenes **1** with an aryl group at the alkyne terminus, the reactant molecules prefer the stepwise over concerted pathway (Scheme 1), passing initially across the high-energy C^2–C^6 transition state **2** ($\Delta G^{\ddagger} \approx 16$–$19$ kcal mol^{-1} at 25 °C, referenced to **1**) into a very shallow minimum harboring the σ,π-diradical intermediate **3** ($\Delta G \approx 12$ kcal mol^{-1} at 25 °C, referenced to **1**). From the singlet intermediate **3** there are two low energy exit channels with free energy barriers of 0.5–2.2 kcal mol^{-1} that lead to the products **6** and **7**, with a direct continuation of momentum from the initial TS.

For the present work, we introduced strong donor substituents in the probing aryl ring in order to fine-tune the system in a way to merge the C^2–C^6 and concerted TSs.

Received: January 9, 2014
Published: March 12, 2014

Scheme 1. C^2–C^6/DA Reaction of Enyne–Allenes (Numbering Started from Alkyne Terminus)

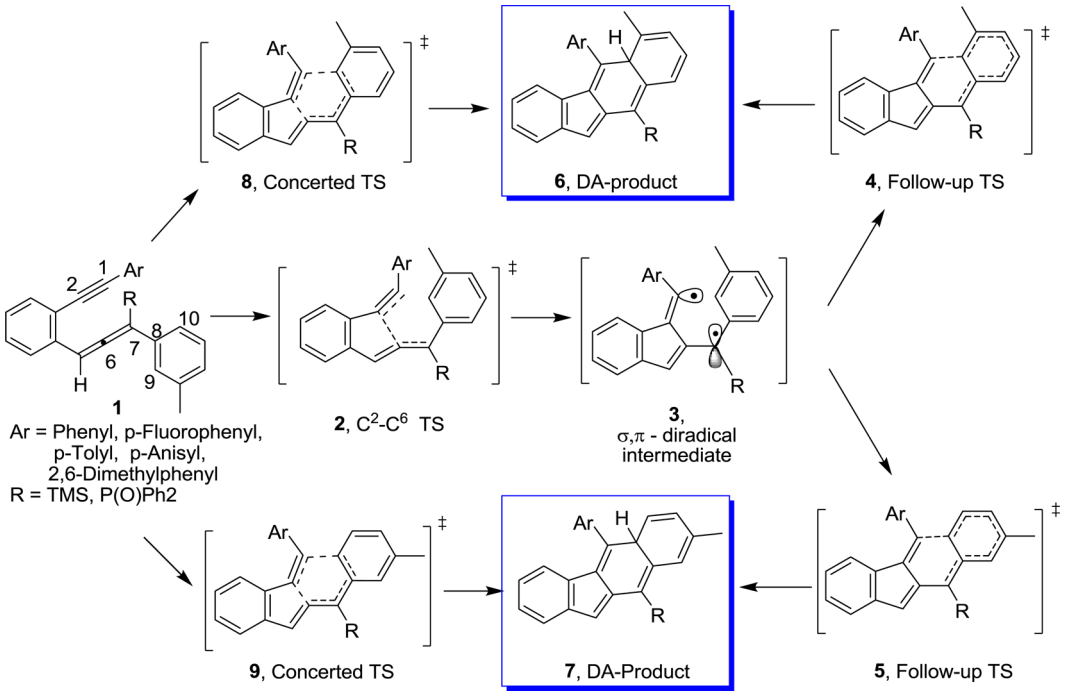

Indeed, we found no separate saddle point for a concerted TS, but two C^2–C^6 TSs that are separated by a significant energy barrier. While the product ratios are no longer temperature independent, the sum of experimental and computational evidence suggests that the enyne–allenes of this study undergo thermal DA cyclization via two distinct stepwise reaction pathways, which share a common intermediate well without mixing. We analyzed the current situation without trajectory computations, relying on DFT-computed $\Delta\Delta G^{\ddagger}$ and experimental product ratios, by developing a straightforward assay that allows to quantify the amount of molecules following nonstatistical dynamics. The results suggest that the percentage of dynamically reacting molecules only slightly depends on the depth of the intermediate well but more on $\Delta\Delta G^{\ddagger}$ of the C^2–C^6 and the follow-up transition states.

RESULTS AND DISCUSSION

Synthesis. In order to address the above mechanistic scenario, we decided to modulate the energy barrier of the second TS in the two-step cyclization while keeping the energy of the initial C^2–C^6 TS and the surface topology as constant as possible. Thus, enyne–allenes **11** were designed with either different groups R or R^1 in a way to generate different degrees of hindrance during rotation of the probing aryl ring. We chose methoxy and *N,N*-dimethylamino substituents as group R and TMS and ^{t}Bu units as R^1. Enyne–allenes **11a–c** were prepared following a reported procedure (Scheme 2).[14] The propargyl acetates[16] **10a,b** were reacted with the corresponding arylmagnesium bromide in the presence of $ZnCl_2$ and Pd(0) to afford **11a–c** in excellent yields.[17]

All compounds were fully characterized by IR, ^{1}H, ^{13}C, and 2D NMR (^{1}H–^{1}H COSY) spectroscopy as well as elemental analysis. Furthermore, formation of the enyne–allenes from the corresponding propargyl acetates was confirmed by following the disappearance of the ^{1}H NMR signal of CH_3CO– at 2.0 ppm and appearance of the highly characteristic carbon signal

Scheme 2. Synthesis of Enyne–Allenes 11a–c

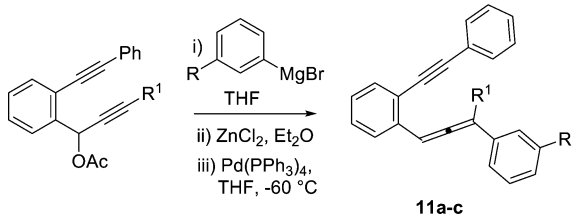

10a R^1 = TMS
10b R^1 = ^{t}butyl

11a-c

		Yield
11a	R = $N(CH_3)_2$, R^1 = TMS	87%
11b	R = OCH_3, R^1 = TMS	92%
11c	R = $N(CH_3)_2$, R^1 = ^{t}butyl	78%

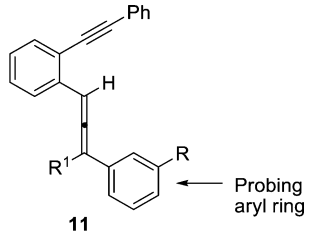

11

of the allene unit (C=C=C) located at ~210 ppm in the ^{13}C NMR spectrum.

Thermolysis. To monitor the effect of temperature on the product ratio, thermolysis of enyne–allenes **11a–c** was performed in dry and degassed toluene at different temperatures using a thermostat operating at a temperature constancy of ±0.1 °C (Scheme 3). Differential scanning calorimetry (DSC) measurements revealed that the onset temperatures of enyne–allenes **11a–c** are in the range of 87–112 °C allowing the thermolysis to be carried out from 30 to 100 °C while maintaining partial conversion. The constitutionally isomeric products **12** and **13** were separated by a long-bed flash column chromatography and characterized with the help of IR, ^{1}H, ^{13}C, and ^{1}H–^{1}H COSY NMR spectroscopy and elemental analysis. In ^{1}H NMR, the main characteristic signal of group R in **12a–c**

dx.doi.org/10.1021/jo500035b | J. Org. Chem. 2014, 79, 2368–2376

Scheme 3. Thermolysis of Enyne–Allenes 11a–c

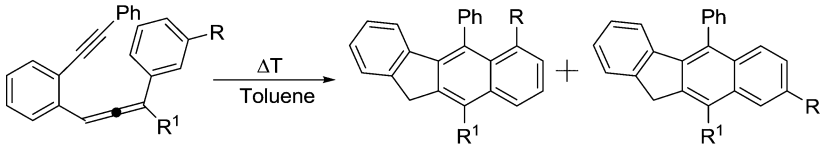

11a-c 12a-c 13a-c

is diagnostically upfield shifted by 0.90–0.46 ppm in comparison to that in **13a–c** because of the adjacent π-electronic shielding effect of the phenyl ring.

Similar to results in another C^2–C^6/DA reaction,[14] in all thermolyses astonishingly the seemingly more hindered product **12** is formed preferentially, a finding that suggests the involvement of nonstatistical dynamics in guiding the product ratio **12**:**13** (Table 1). However, in all present cases, the product ratio is not temperature independent, at first a seemingly convincing argument not to consider nonstatistical dynamics. Indeed, thermolysis of **11b,c** shows a continuous decrease in the product ratio **12**/**13** when increasing the temperature from 30 to 100 °C. Differently, the ratio **12a**/**13a** first augments from 1.48 to 1.65 in the temperature range from 30 to 60 °C but then equally decreases continuously with increasing temperature.

Table 1. Experimental Product Ratios 12:13 in the Thermolysis of Enyne–Allenes 11a–c

compd[a]	temp (°C)	time (min)	exptl ratio[b] **12**:**13**	nonstatistical dynamics[c] (%)
11a	30	1020	1.48:1	71
	40	780	1.62:1	75
	50	420	1.64:1	76
	60	180	1.65:1	76
	70	75	1.62:1	76
	80	70	1.60:1	76
	90	50	1.58:1	76
	100	40	1.56:1	76
11b	30	1020	1.72:1	71
	40	780	1.69:1	72
	50	420	1.66:1	72
	60	180	1.64:1	72
	70	75	1.63:1	72
	80	70	1.61:1	72
	90	50	1.57:1	73
	100	40	1.54:1	74
11c	40	720	2.50:1	85
	50	420	2.46:1	86
	60	180	2.38:1	85
	70	75	2.29:1	85
	80	70	2.21:1	84
	90	50	2.11:1	83
	100	30	2.06:1	83

[a] T_{onset} (DSC) = 90 °C (**11a**), 87 °C (**11b**), and 112 °C (**11c**). [b] Ratios were determined from the proton NMR spectrum of the crude product after thermolysis with experimental accuracy of ±0.03. [c] Calculated using eqs 1 and 2.

Computation. To evaluate the positional selectivity and the origin of the temperature dependence of the product ratio **12**:**13** in the thermal cyclization, reaction profiles were computed using DFT as implemented in the Gaussian 09 program package.[18] The unrestricted Becke pure gradient-corrected exchange functional, in conjunction with the Lee–Yang–Parr nonlocal correlation functional (BLYP)[19] using the moderate 6-31G* basis set[20] along with broken spin symmetry (involving the mixing of the HOMO and LUMO to break the spin and spatial symmetries), was found to generate rather reliable results in Schmittel (C^2–C^6) and Myers–Saito (C^2–C^7) cyclizations of enyne–allenes as documented by Schreiner et al..[21] Therefore, we utilized the (BS)-UBLYP method in conjunction with the 6-31G* basis set to optimize all stationary points in the gas phase. Calculated minima and first-order saddle point structures were verified by analyzing their harmonic vibrational frequencies via their analytical second derivatives (NIMAG = 0 and 1, respectively). Free energies including unscaled zero-point vibrational energies after thermal correction are given in kcal mol^{-1} relative to the corresponding starting materials. All TSs were optimized using the qst2 and qst3 method as implemented in Gaussian 09 and the lowest energy TSs were taken into consideration in each case. Free energy values at 25 °C are provided for all stationary points of the cyclization of **11a–c** (Figure 1). A thermochemical analysis of the optimized structures at different temperatures reveals that the free energy differences are insignificant within 30–100 °C.

The computed reaction profiles of **11a–c** (Figure 1) confirm a stepwise thermal cyclization via the diradical **11a-cINT** as the minimum energy path (MEP). For all systems, the free energy of the C^2–C^6 TSs is higher than that of follow-up TSs; hence, according to TST the C^2–C^6 TS is the rate-limiting step and the second TS the product-determining step. Notably, though, the computed data on the final ring closure of the diradical, see **11aTS2**‡, **11cTS2**‡ vs **11aTS2′**‡, **11cTS2′**‡, predict a preferential formation of the less hindered products **13a** and **13c**, quite in contrast to the experimental outcome. Such finding is not in line with TST but may hint the involvement of nonstatistical dynamics in the product formation. In contrast, the preferential formation of the more hindered product **12b** is predicted by the computational data, but there is a large discrepancy between experimental and computed ratio.

To obtain further insight, partial potential energy surfaces (PES) were computed for enyne–allene **11a** (Figures 2 and 3). The first PES was obtained by varying the C2–C6 distance and C6–C7–C8–C9 dihedral angle sampling 221 points (13 × 17) at the (BS)-UBLYP/6-31G* level (Figure 2). It shows a broad single well for the diradical intermediate with the energy only raising by 0.35 kcal mol^{-1} above the lowest energy point when the dihedral angle C6–C7–C8–C9 changes between 70 and 125° (Figure 4, left). Interestingly, the two initial C^2–C^6 TSs on the PES, **11aTS1**‡ and **11aTS1′**‡, are separated by a significant energy barrier of ca. 5.85 kcal mol^{-1} (observed from **11aTS1**‡ in the PES scan, Figure 2). The C6–C7–C8–C9 dihedral angle was initially chosen to encompass all of the stationary points in one surface, but the scan started to produce an erroneous warping near the second TSs. In order to avoid problems with the surface topology, we chose the C2–C6 and

dx.doi.org/10.1021/jo500035b | J. Org. Chem. 2014, 79, 2368–2376

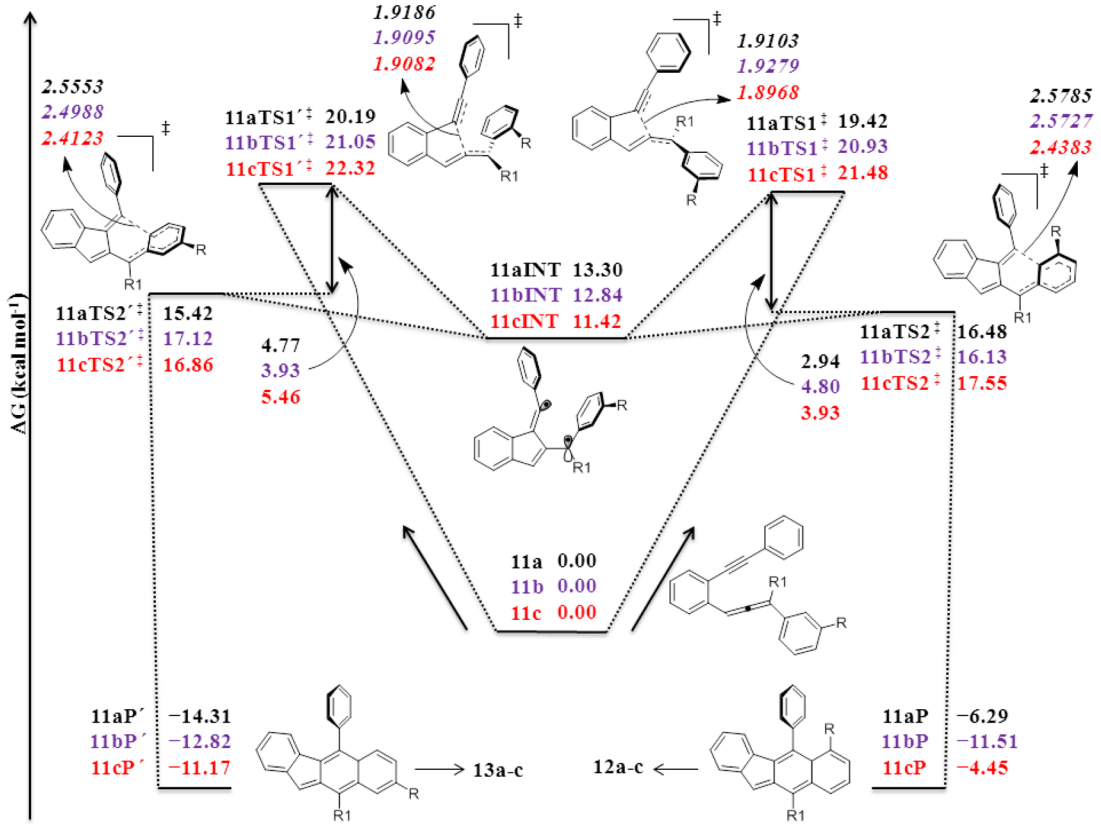

Figure 1. Reaction profile for the thermal cyclization of **11a−c** in the gas phase at the (BS)-(U)/BLYP/6-31G(d) level. Bond distances (Å) are shown in italics, and relative free energies at 25 °C are given in kcal mol^{-1}. Numerical values in black, blue, and red correspond to **11a**, **11b**, and **11c**. **TS1** and **TS2** refer to the initial C^2−C^6 and diradical closure transitions states, respectively, and **INT** to the diradical intermediate. The primed designations relate to attack at the less hindered aromatic position of the probing ring.

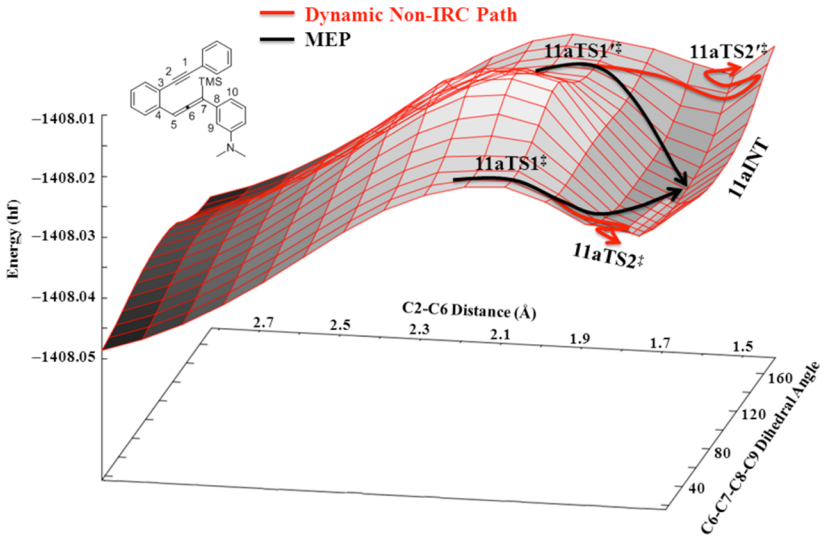

Figure 2. 2D relaxed potential energy surface scan of C2−C6 distance from 2.8 to 1.4 Å with respect to C6−C7−C8−C9 dihedral angle from 16 to 176° (0.1 Å × 10° grid size).

C1−C10 distances for a second surface scan (Figure 3). The C2−C6 distance was decreased from 2.5 to 1.2 Å and the C1−C10 distance from 3.7 to 1.3 Å with the step size of 0.1 Å in both cases. This partial PES reveals the topology about the Diels−Alder product **11aP′** encompassing additionally the stationary points **11aTS1′**‡, **11aTS2′**‡, and **11aINT**.

Transition state **11aTS1′**‡ (ΔG = 20.19 kcal mol^{-1}) is 0.77 kcal mol^{-1} higher in energy than **11aTS1**‡ (ΔG = 19.42 kcal mol^{-1}). The two follow-up TSs, **11aTS2**‡ and **11aTS2′**‡, connecting the product to the diradical intermediate were also located. Here, the situation is inverted with transition state **11aTS2′**‡ (ΔG = 15.42 kcal mol^{-1}) being 1.06 kcal mol^{-1} lower in energy than **11aTS2**‡ (ΔG = 16.48 kcal mol^{-1}). Accordingly, diradical **11aINT** being located at 13.30 kcal mol^{-1} in a shallow well, is separated from products **11aP** and **11aP′** by small barriers $\Delta G^{‡}$ = 3.18 and 2.12 kcal mol^{-1},

dx.doi.org/10.1021/jo500035b | J. Org. Chem. 2014, 79, 2368−2376

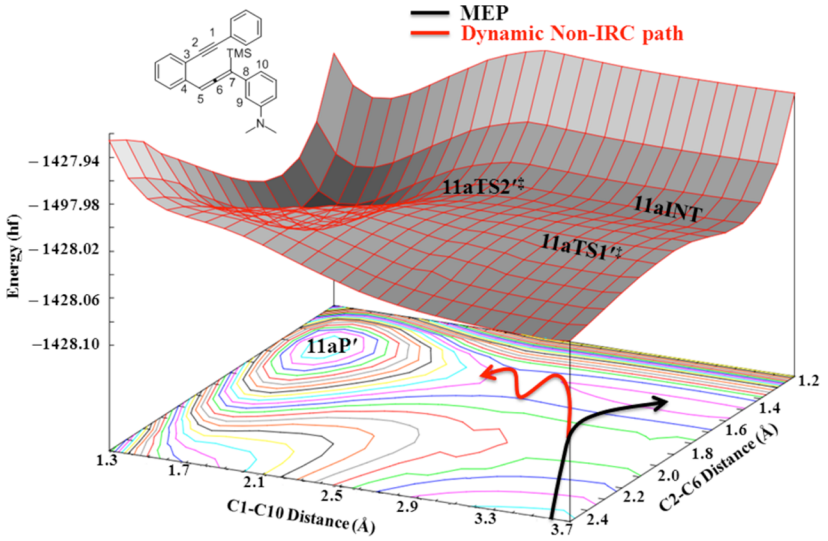

Figure 3. 2D relaxed potential energy surface and corresponding contour plot generated by the scan of C2−C6 distance from 2.5 to 1.2 Å with respect to C1−C10 distance from 1.3 to 3.7 Å (0.1 Å × 0.1 Å grid size).

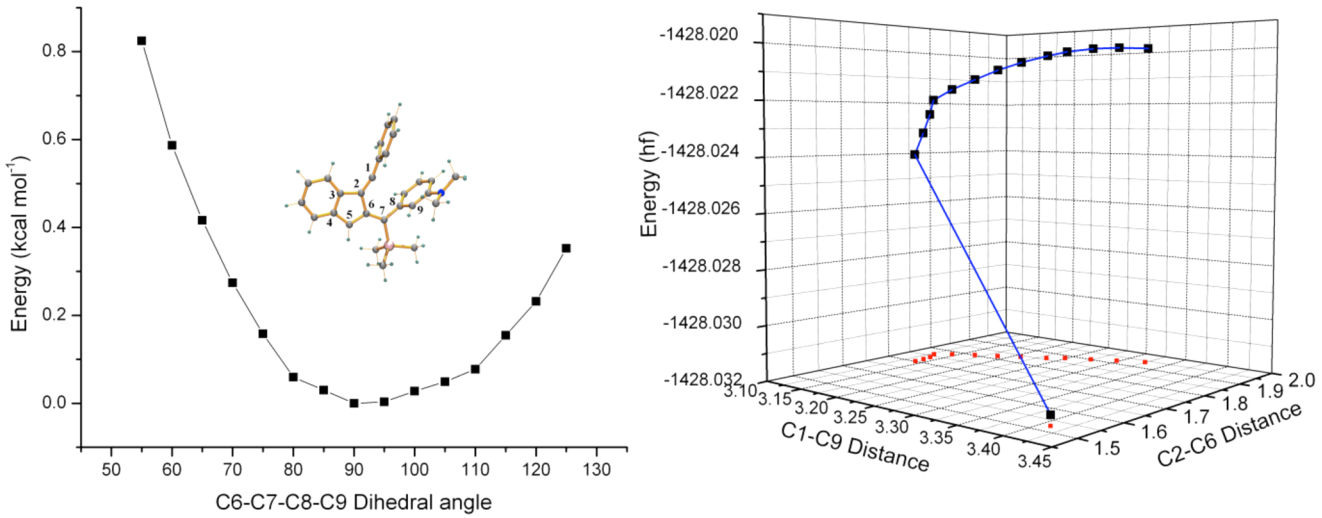

Figure 4. 1D scan of C6−C7−C8−C9 dihedral angle keeping the C2−C6 distance fixed at 1.52 Å which is the intermediate distance (left side). 1D scan of C2−C6 distance from 1.94 to 1.70 Å with 0.02 Å interval (right side). Red dots are the projection of the black points on the plane counting for two distance coordinates.

respectively, suggesting preferential formation of **13a** via **11aP′**. Clearly, the experimental finding with **12a** formed preferentially over **13a** is not in accord with a TST-controlled product formation from the singlet intermediate **11aINT**. According to the computations, a concerted pathway can also be excluded because no concerted TS for **11aP** was located; each attempt afforded the optimized initial C^2−C^6 TS. Likewise, the PES (Figure 3) does not show any separate saddle on the surface corresponding to direct conversion to **11aP′**. Summing up the experimental and computational results on **11a** there is an apparent difficulty to explain the results in a consistent manner using TST.

A more detailed analysis of the surface (Figure 3, black arrow) reveals that the MEP starting from **11aTS1′**‡ leads initially to a decreasing but later to an increasing C1−C10 distance on the way to diradical intermediate **11aINT**. Therefore, the MEP toward the intermediate involves a brusque bending on the surface. In general, after crossing a TS, molecules transform their potential energy into kinetic energy while following the reaction coordinate along the *steepest descent path*. Here, however, the bend of the MEP requires a sudden reversal of momentum of all atoms to reach the diradical minimum. As any bent path is very difficult to follow by molecules that have enough kinetic energy, they will rather continue their initial momentum and even cross follow-up barrier(s) if their kinetic energy is sufficient.

Although the PES toward formation of **11aP** was not determined with respect to C2−C6 and C1−C9 distance coordinates, the PES with respect to the C2−C6 distance and C6−C7−C8−C9 dihedral angle (Figure 2) equally showed a bending in the MEP toward formation of **11aINT** after crossing **11aTS1**‡. A better visualization of the bending is provided by a 1D scan of the C2−C6 distance from 1.94 to 1.70 Å at 0.02 Å intervals (Figure 4, right) revealing the C1−C9 distance to decrease initially from 3.40 Å (at **11aTS1**‡, Figure 5) to 3.13 Å when the C2−C6 bond distance approaches 1.76 Å. At that point, the C1−C9 distance starts to lengthen, finally affording the intermediate with a C1−C9 distance at 3.41 Å. If dynamics

dx.doi.org/10.1021/jo500035b | J. Org. Chem. 2014, 79, 2368−2376

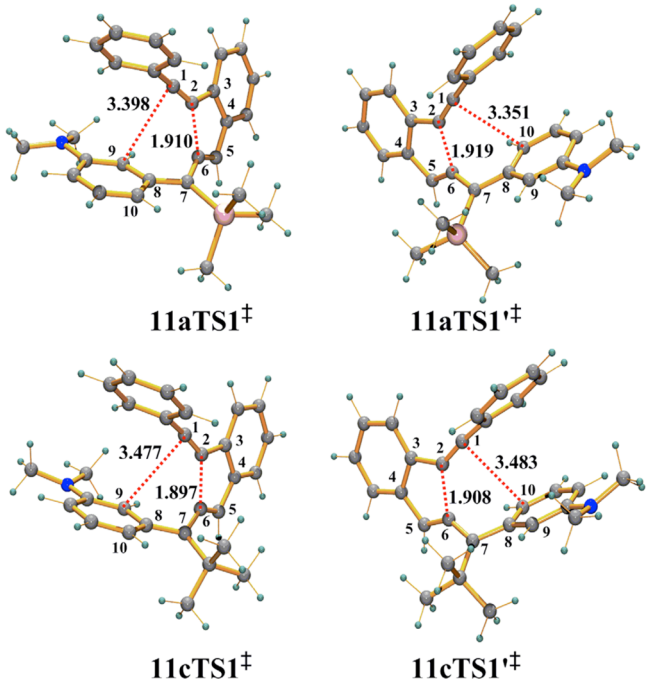

Figure 5. Optimized TSs, **11aTS1**‡, **11aTS1′**‡, **11cTS1**‡, and **11cTS1′**‡ with distances in angstroms.

plays a role after crossing the initial TS, **11aTS1**‡, then one would expect the product to form in a direct continuation of the primary momenta of atoms C1 and C9. In such case, the decrease of the C1−C9 distance would continue even after reaching a C2−C6 bond distance of 1.76 Å leading to a deviation from the MEP. On the other hand, increasing the C1−C9 distance along the calculated MEP as shown in Figure 4 (right) will lead to a loss of the momenta of atoms C1 and C9, thus enforcing a TST-controlled product formation.

Molecules that originally cross **11aTS1**‡ have little probability to produce **11aP′** if they are not relaxed in the intermediate well because the required large change of the C6−C7−C8−C9 dihedral angle has to be a sluggish process due to the resultant large movement of a considerable number of atoms. Such a process needs vibrational energy redistribution in the intermediate during the overall process **11aTS1**‡ → **11aP′**.

To sumarize the results from inspecting the PES, a certain fraction of the molecules crossing the transition state **11aTS1**‡ will go to product **11aP** directly under dynamic control, while the remaining fraction of molecules will relax vibrationally in the intermediate well. The relaxed molecules will statistically partition to produce both **11aP** and **11aP′** according to the two follow-up TSs **11aTS2**‡ and **11aTS2′**‡. Similarly, those molecules passing initially through **11aTS1′**‡ will produce **11aP′** preferably in a nonstatistical dynamic scenario. Assuming a nonstatistical setting on the basis of PES considerations may seem daring, but in related C^2−C^6 cyclizations, various pieces of evidence, such as temperature-independent product ratios,[14] intra- and intermolecular kinetic isotope effects,[5a,13] and trajectory computations,[13] have substantiated the occurrence of nonstatistical dynamics.

Considering a dynamic model, a huge number of dynamic trajectory calculations would be necessary to describe the motion, momenta, and fraction of molecules following nonstatistical dynamics. Thus, one would like to reduce the costs of the molecular dynamics computations by turning to simplified model systems, but clearly in the present case each substituent at the enyne−allenes matters.

Apart from costly dynamic trajectory computations, other protocols, such as the canonical competitive nonstatistical model (CCNM) by Truhlar[22] and the RRKM-Master equation as elaborated by Glowacki,[8d,23] equally allow rationalization of the branching in nonstatistical reactions, although their validity is still under scrutiny.[3d] Our protocol,[24] in contrast, offers a very simple way to approximate the fraction of molecules that follow nonstatistical dynamics by comparing the experimental ratios with the statistical partitioning as follows:

$$X_{ns}Q_1 + X_sQ_2 = Q_{exp} \quad (1)$$

$$X_{ns} + X_s = 1 \quad (2)$$

Here, X_{ns} = mole fraction of molecules following the nonstatistical (ns) dynamically controlled pathway; X_s = mole fraction of molecules following the statistically (s) controlled pathway; Q_1 = partitioning created at the initial (C^2−C^6) TSs; Q_2 = partitioning created at the second TSs; Q_{exp} = experimental product ratio.

In the thermolysis of enyne−allene **11a**, for instance, the experimentally observed product ratio **12a**:**13a** is 1.48:1 at 30 °C. If all molecules continued with conservation of momentum through the diradical well after crossing the two initial C^2−C^6 TSs, **11aTS1**‡ and **11aTS1′**‡, then according to computational results the observed product ratio would be 3.63:1 ($\Delta\Delta G^{‡}$ = 0.77 kcal mol^{-1}). Using eqs 1 and 2, 29% of the reacting molecules do not follow dynamic behavior in the intermediate, but instead partition in a ratio of 1:6.25 to afford **11aP** (4%) and **11aP′** (25%). With higher temperature, the percentage of molecules following nonstatistical dynamics increases very slightly from 71% (30 °C) to 76% (50 °C) but then remains almost constant up to 100 °C.

In order to test our theoretical model in another system, we chose a methoxy group as R in the probing aryl ring of **11b**. Surprisingly, while the two initial TSs, **11bTS1**‡ and **11bTS1′**‡, are located at similar free energies of 20.93 and 21.05 kcal mol^{-1} (at 25 °C), respectively, the relative free energy of the follow-up TSs favors formation of the more hindered product via **11bTS2**‡ at 16.13 kcal mol^{-1}, which is 0.99 kcal mol^{-1} lower than that of **11bTS2′**‡. The structural origin favoring the more hindered product (Figure 6) is hidden in the C2−C1−C11−C12 dihedral angle of **11bTS2**‡ and **11bTS2′**‡. Since the phenyl ring at the alkyne terminus provides stabilization to the reacting σ-radical site, any deviation of the C2−C1−C11−C12 dihedral angle from 90° will destabilize the system. In **11bTS2′**‡, the dihedral angle deviates by 18.5°, which is more than in **11bTS2**‡ with a deviation of only 7.1°. As one would expect, the longer C1−C9 bond distance (2.57 Å) in **11bTS2**‡ allows the C2−C1−C11−C12 angle to stay closer to 90°. In contrast, despite the C1−C9 and C1−C10 bond distances in **11aTS2**‡ and **11aTS2′**‡, respectively, being rather long at 2.58 and 2.56 Å, the C2−C1−C11−C12 dihedral angle deviates more in **11aTS2**‡ (by 25.1°) than in **11aTS2′**‡ (by 15.1°) due to excessive steric repulsion between the *N*,*N*-dimethylamino and the adjacent phenyl group in the former.

In accordance with TST, one would expect a product ratio **12b**:**13b** of 5.18:1 (calculated $\Delta\Delta G^{‡}$ = 0.99 kcal mol^{-1}) at 30 °C, but we observe only a ratio of 1.72:1, which is rather close to the partitioning at the initial TSs (1.22:1 as derived from $\Delta\Delta G^{‡}$ = 0.12 kcal mol^{-1}). The large deviation from the TST-predicted ratio provides some support for the occurrence of

dx.doi.org/10.1021/jo500035b | J. Org. Chem. 2014, 79, 2368−2376

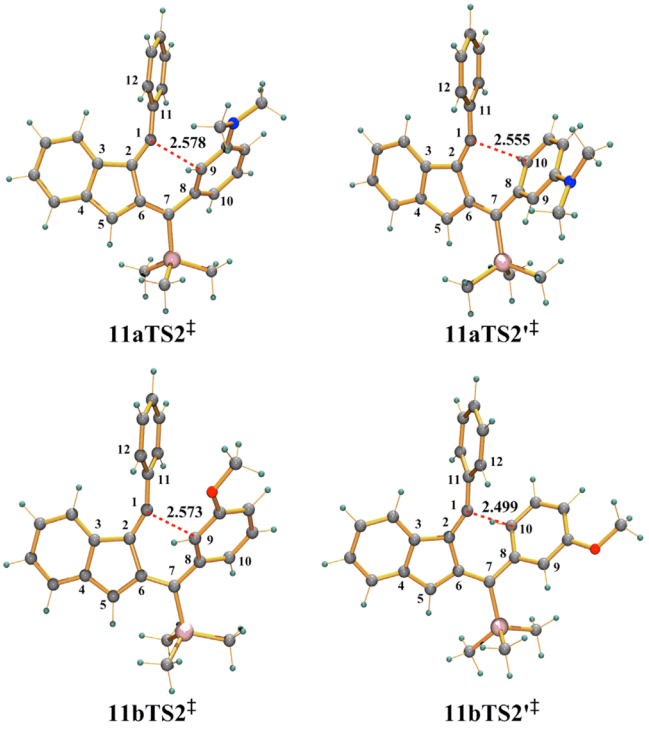

Figure 6. Optimized TSs, **11aTS2**‡, **11aTS2′**‡, **11bTS2**‡, and **11bTS2′**‡ with distances given in angstroms.

nonstatistical dynamic behavior equally in this case. In comparison with enyne-allene **11a**, the depth of the intermediate well in the reaction of **11b** is more pronounced thus opposing dynamics although due to the initial, higher energy C^2-C^6 TSs more kinetic energy should be available for molecules on the downhill side. These two opposing effects in summary provide a little less dynamic system (71−74% nonstatistical dynamics) using eqs 1 and 2.

In order to generate an even deeper well at the intermediate, we replaced the trimethylsilyl with a *tert*-butyl group at the allene terminus. This suggestion emerged from the computed energy profile about the dihedral angle in a model benzyl radical (Figure 7) revealing that the rotation of an adjacent aryl ring is sterically less hindered with a trimethylsilyl than a *tert*-butyl group due to the longer C−Si bond distance. Thus, enyne−allene **11c** was prepared and studied. Figure 7 shows a double-minimum profile for the TMS-substituted molecule, while only a single minimum for the intermediate well (**11aINT** and **11bINT**) of enyne-allenes **11a,b** is observed.

In case of enyne−allene **11c**, the singlet intermediate **11cINT** is placed at 11.42 kcal mol^{-1} and the two follow-up TSs, **11cTS2**‡ and **11cTS2′**‡, are located at 17.55 and 16.86 kcal mol^{-1}. The follow-up TSs, **11cTS2**‡ and **11cTS2′**‡, are thus 1.07 and 1.44 kcal mol^{-1} higher in energy than those of **11aTS2**‡ and **11aTS2′**‡, respectively, whereas **11cINT** is lower in energy than **11aINT** (13.30 kcal mol^{-1}). Clearly, the cyclization of enyne−allene **11c** proceeds through a much deeper energy well for the diradical intermediate. Surprisingly, though, the percentage of dynamically reacting molecules is much higher (83−86%) for **11c** than for **11a,b**. A closer analysis of the stationary points reveals significantly longer bond distances in **11cTS1**‡ (d_{C1-C9} = 3.48 Å) and **11cTS1′**‡ (d_{C1-C10} = 3.48 Å), respectively, than in **11aTS1**‡ (d_{C1-C9} = 3.40 Å) and **11aTS1′**‡ (d_{C1-C10} = 3.35 Å) indicating that the C^2-C^6 TSs of **11c** are more displaced from the product

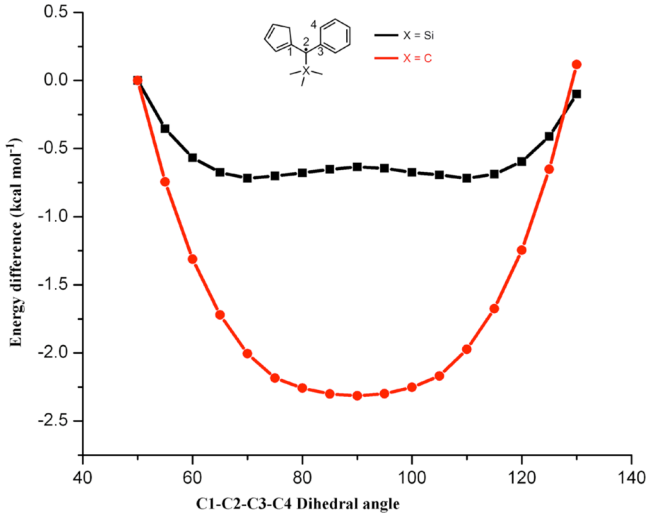

Figure 7. 1D scan of C1−C2−C3−C4 dihedral angle of the (cyclopenta-1,3-dien-1-yl)trimethylsilylbenzyl radical and (cyclopenta-1,3-dien-1-yl)-*tert*-butylbenzyl radical using the UBLYP/6-31G* method.

structure than the TSs of **11a** (Figure 5). As a result, the two C^2-C^6 TSs, **11cTS1**‡ and **11cTS1′**‡, are 2.06 and 2.13 kcal mol^{-1} higher in energy than those of **11aTS1**‡ and **11aTS1′**‡, respectively, and the free energy differences $\Delta\Delta G^{\ddagger}$ for **11aTS1**‡→**11aTS2**‡, **11aTS1′**‡→**11aTS2′**‡, **11cTS1**‡→**11cTS2**‡, and **11cTS1′**‡→**11cTS2′**‡ are −2.94, −4.77, −3.93, and −5.46 kcal mol^{-1}, respectively. These values indicate that, in the case of **11c**, the molecules receive much more kinetic energy after passage through the initial TSs so that overcoming the second TSs is easier, generating more dynamically reacting molecules in comparison to enyne−allene **11a**.

In systems **11a,c**, we thus see an increasing contribution of nonstatistically reacting molecules with increasing free energy gap between the initial TS and second TS. The higher fraction of dynamically reacting molecules in **11c**, despite a much deeper intermediate well, suggests that the well depth in systems with PES such as in Figure 2 is not the decisive factor determining the amount of nonstatistical dynamics.

Nonstatistical Dynamic vs Asynchronous Concerted Reaction Path. Finally, one needs to ask whether the above suggested nonstatistical dynamic reaction course is any different from a largely asynchronous concerted one. According to IUPAC, a concerted reaction is a single-step reaction through which reactants are directly transformed into products without involvement of any intermediates. But would this definition still be of utility when the intermediate zone is passed only at the rim with conservation of momentum?

An asynchronous concerted reaction is realized as a two-stage reaction in which the changes in bonding occur in two distinct stages, some changes mainly taking place between the reactant and transition state, the others mainly between the transition state and product.[25] For example, **11aTS′**‡ could indeed serve for a highly asynchronous concerted reaction path if the trajectories would exclusively develop along *the ridge* that is depicted as a blue line in Figure 8. Despite the principal possibility, the highly asynchronous concerted reaction path seems to be very unlikely as the initial TS exhibits no displacement amplitude toward C1−C10 bond formation in the imaginary frequency. Rather, it describes almost exclusively the C2−C6 displacement. Hence, the more like scenario

dx.doi.org/10.1021/jo500035b | J. Org. Chem. 2014, 79, 2368−2376

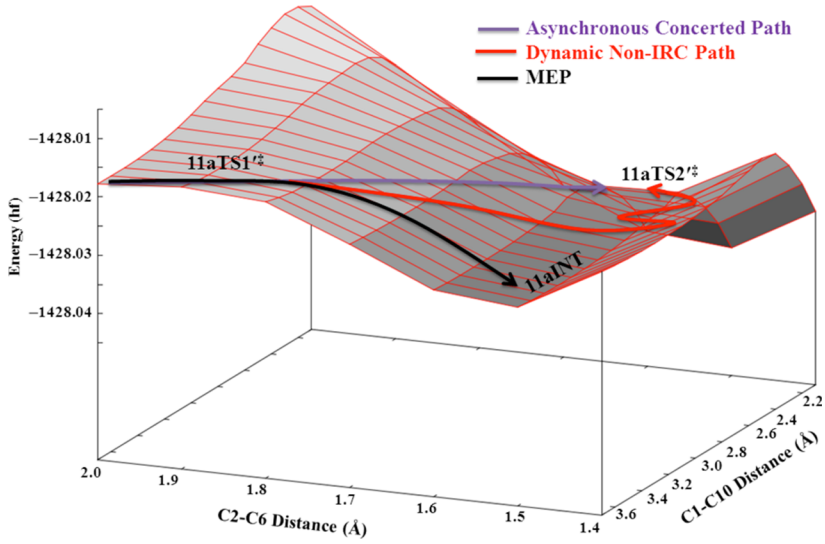

Figure 8. 2D potential energy surface generated by scanning the C2−C6 distance from 2.0 to 1.4 Å and the C1−C10 distance from 2.1 to 3.7 Å (0.1 Å × 0.1 Å grid size) (truncated Figure 3).

demands that after crossing the initial TS, a C2−C6 bond quickly forms subsequently supporting C1−C10 bond formation by maintaining the initial momentum. Finally, a nonstatistical dynamic course (red line in Figure 8) evolves for the reaction.

In summary, we present three closely related enyne−allenes that follow a stepwise mechanism for their thermal cyclization. According to an inspection of the PES, two noninteracting reaction paths share a common intermediate well without losing memory of their previous transition-state passage resulting preferentially in a nonstatistical dynamic behavior. An equation connecting $\Delta\Delta G^{\ddagger}$ of the first and second transition states with the experimentally determined product ratio allows us to calculate the amount of nonstatistical dynamics in the overall process, a method that could also be of use in other systems. The thus-determined percentage of dynamically reacting molecules only slightly depends on the depth of the intermediate well but rather more on $\Delta\Delta G^{\ddagger}$ between the initial and the follow-up transition states.[26] Such findings should raise the awareness toward the importance of *conservation of momentum*[15a] and of nonstatistical dynamics in reaction mechanisms.

Moreover, the present results suggest that nonstatistical dynamics may even influence systems that do not show the typical phenomena, which are often associated with nonstatistical behavior, such as special kinetic isotope effects,[5a,13,27] temperature-independent product ratios,[14,15b] or inversion of configuration in rearrangements of strained systems.[28]

■ ASSOCIATED CONTENT

Supporting Information

Synthetic and experimental procedures are described in addition to spectroscopic and computational data. This material is available free of charge via the Internet at http://pubs.acs.org.

■ AUTHOR INFORMATION

Corresponding Author

*E-mail: schmittel@chemie.uni-siegen.de.

Notes

The authors declare no competing financial interest.

■ ACKNOWLEDGMENTS

We are indebted to the Deutsche Forschungsgemeinschaft for financial support and to Prof. Jaquet (Siegen) for helpful support concerning the computational infrastructure.

■ REFERENCES

(1) (a) Eyring, H. *J. Chem. Phys.* **1935**, *3*, 107. (b) Wigner, E. *Trans. Faraday Soc.* **1938**, *34*, 29.

(2) (a) Kassel, L. S. *Chem. Rev.* **1932**, *10*, 11. (b) Rice, O. K.; Ramsperger, H. C. *J. Am. Chem. Soc.* **1927**, *49*, 1617. (c) Marcus, R. A. *J. Chem. Phys.* **1952**, *20*, 352. (d) Marcus, R. A. *J. Chem. Phys.* **1952**, *20*, 355.

(3) (a) Doubleday, C.; Li, G.; Hase, W. L. *Phys. Chem. Chem. Phys.* **2002**, *4*, 304. (b) Thomas, J. B.; Waas, J. R.; Harmata, M.; Singleton, D. A. *J. Am. Chem. Soc.* **2008**, *130*, 14544. (c) Rehbein, J.; Carpenter, B. K. *Phys. Chem. Chem. Phys.* **2011**, *13*, 20906. (d) Carpenter, B. K. *Chem. Rev.* **2013**, *113*, 7265.

(4) (a) Sun, L.; Song, K.; Hase, W. L. *Science* **2002**, *296*, 875. (b) Bogle, X. S.; Singleton, D. A. *Org. Lett.* **2012**, *14*, 2528.

(5) (a) Schmittel, M.; Vavilala, C.; Jaquet, R. *Angew. Chem., Int. Ed.* **2007**, *46*, 6911. (b) Lan, Y.; Danheiser, R. L.; Houk, K. N. *J. Org. Chem.* **2012**, *77*, 1533.

(6) (a) Nummela, J. A.; Carpenter, B. K. *J. Am. Chem. Soc.* **2002**, *124*, 8512. (b) Zhou, J.; Schlegel, H. B. *Theor. Chem. Acc.* **2012**, *131*, 1126.

(7) (a) Bach, A.; Hostettler, J. M.; Chen, P. *J. Chem. Phys.* **2006**, *125*, 024304. (b) Broyles, D. A.; Carpenter, B. K. *Org. Biomol. Chem.* **2005**, *3*, 1757. (c) Gasser, M.; Bach, A.; Chen, P. *Phys. Chem. Chem. Phys.* **2008**, *10*, 1133. (d) Gasser, M.; Frey, J. A.; Hostettler, J. M.; Bach, A. *Chem. Commun.* **2011**, *47*, 301. (e) Matute, R. A.; Houk, K. N. *Angew. Chem., Int. Ed.* **2012**, *51*, 13097.

(8) (a) Katori, T.; Itoh, S.; Sato, M.; Yamataka, H. *J. Am. Chem. Soc.* **2010**, *132*, 3413. (b) Itoh, S.; Yamataka, H. *Chem.—Eur. J.* **2011**, *17*, 1230. (c) Itoh, S.; Yoshimura, N.; Sato, M.; Yamataka, H. *J. Org. Chem.* **2011**, *76*, 8294. (d) Goldman, L. M.; Glowacki, D. R.; Carpenter, B. K. *J. Am. Chem. Soc.* **2011**, *133*, 5312. (e) Akimoto, R.; Tokugawa, T.; Yamamoto, Y.; Yamataka, H. *J. Org. Chem.* **2012**, *77*, 4073.

(9) (a) Schmittel, M.; Strittmatter, M.; Kiau, S. *Tetrahedron Lett.* **1995**, *36*, 4975. (b) Schmittel, M.; Steffen, J.-P.; Rodríguez, D.; Engelen, B.; Neumann, E.; Cinar, M. E. *J. Org. Chem.* **2008**, *73*, 3005. (c) Schmittel, M.; Vavilala, C.; Cinar, M. E. *J. Phys. Org. Chem.* **2012**, *25*, 182.

(10) (a) Schmittel, M.; Kiau, S.; Siebert, T.; Strittmatter, M. *Tetrahedron Lett.* **1996**, *37*, 7691. (b) Schmittel, M.; Maywald, M.; Strittmatter, M. *Synlett* **1997**, 165.

(11) (a) Zhang, H. -R.; Wang, K. K. *J. Org. Chem.* **1999**, *64*, 7996. (b) Wang, K. K.; Zhang, H.-R.; Petersen, J. L. *J. Org. Chem.* **1999**, *64*, 1650. (c) Dai, W.; Petersen, J. L.; Wang, K. K. *Org. Lett.* **2006**, *8*, 4665. (d) Zhang, Y.; Petersen, J. L.; Wang, K. K. *Org. Lett.* **2007**, *9*, 1025. (e) Cinar, M. E.; Vavilala, C.; Fan, J.; Schmittel, M. *Org. Biomol. Chem.* **2011**, *9*, 3776.
(12) (a) Schmittel, M.; Steffen, J.-P.; Wencesla, M. Á.; Engels, B.; Lennartz, C.; Hanrath, M. *Angew. Chem., Int. Ed.* **1998**, *37*, 1562. (b) Schmittel, M.; Rodríguez, D.; Steffen, J.-P. *Molecules* **2000**, *5*, 1372.
(13) Bekele, T.; Christian, C. F.; Lipton, M. A.; Singleton, D. A. *J. Am. Chem. Soc.* **2005**, *127*, 9216.
(14) Samanta, D.; Cinar, M. E.; Das, K.; Schmittel, M. *J. Org. Chem.* **2013**, *78*, 1451.
(15) (a) Carpenter, B. K. *J. Am. Chem. Soc.* **1985**, *107*, 5730. (b) Carpenter, B. K. *Acc. Chem. Res.* **1992**, *25*, 520.
(16) Fleming, I.; Terrett, N. K. *J. Organomet. Chem.* **1984**, *264*, 99.
(17) Elsevier, C. J.; Stehouwer, P. M.; Westmijze, H.; Vermeer, P. *J. Org. Chem.* **1983**, *48*, 1103.
(18) Frisch, M. J. et al. *Gaussian 09, Revision A.1*; Gaussian, Wallingford, CT, 2009.
(19) (a) Becke, A. D. *Phys. Rev. A* **1988**, *38*, 3098. (b) Lee, C.; Yang, W.; Parr, R. G. *Phys. Rev. B* **1988**, *37*, 785.
(20) (a) Ditchfield, R.; Hehre, W. J.; Pople, J. A. *J. Chem. Phys.* **1971**, *54*, 724. (b) Hehre, W. J.; Ditchfield, R.; Pople, J. A. *J. Chem. Phys.* **1972**, *56*, 2257. (c) Hariharan, P. C.; Pople, J. A. *Theoret. Chim. Acta* **1973**, *28*, 213.
(21) Prall, M.; Wittkopp, A.; Schreiner, P. R. *J. Phys. Chem. A* **2001**, *105*, 9265.
(22) Zheng, J.; Papajak, E.; Truhlar, D. G. *J. Am. Chem. Soc.* **2009**, *131*, 15754.
(23) Glowacki, D. R.; Liang, C. H.; Marsden, S. P.; Harvey, J. N.; Pilling, M. J. *J. Am. Chem. Soc.* **2010**, *132*, 13621.
(24) The outcome of this model largely depends on the accuracy of the computed free energy barriers.
(25) Dewar, M. J. S.; Pierini, A. B. *J. Am. Chem. Soc.* **1984**, *106*, 203.
(26) (a) Quijano, L. M. M.; Singleton, D. A. *J. Am. Chem. Soc.* **2011**, *133*, 13824. (b) Oyola, Y.; Singleton, D. A. *J. Am. Chem. Soc.* **2009**, *131*, 3130.
(27) Andujar-De Sanctis, I. L.; Singleton, D. A. *Org. Lett.* **2012**, *14*, 5238.
(28) Schmittel, M.; von Seggern, H. *J. Am. Chem. Soc.* **1993**, *115*, 2165.